AIAA 82-4110

# Fully Laminar Flow Airfoil Sections

J. Sapuppo*
*University of New South Wales, Sydney, Australia*
and
R.D. Archer†
*United States Naval Academy, Annapolis, Md.*

**Fully laminar flow airfoil shapes have been designed using the appropriate Stratford pressure gradient criterion. Large nose radius is required. Maximum tolerable thickness was 10% at about 15% chord. Maximum tolerable camber was 10% at 15% chord with very low usable ranges of angle of attack and lift coefficient. Flow visualization has confirmed the presence of laminar flow over the whole chord on a wind-tunnel model.**

## Nomenclature

| | |
|---|---|
| $C_\ell$ | = section lift coefficient |
| $C_p$ | = pressure coefficient |
| $\bar{C}_p$ | = canonical pressure coefficient |
| $\ell$ | = lift of an airfoil section, force per unit span |
| $p$ | = pressure |
| $p_0$ | = peak pressure on upper surface of section |
| $Re$ | = Reynolds number based on section chord |
| $s, s_p$ | = airfoil surface length coordinate, stagnation point, Fig. 1 |
| $s$ | = surface length, magnitude $s$ |
| $t/c$ | = thickness, chord ratio |
| $T$ | = turbulence level of airstream |
| $v$ | = velocity, magnitude $v$ |
| $v$ | = local airfoil surface velocity |
| $v_\ell(s), v_u(s)$ | = velocity distribution on lower/upper surface of section |
| $v_0$ | = peak velocity on upper surface, Figs. 2 and 3 |
| $V_\infty$ | = freestream velocity—assigned a value of unity |
| $x, \bar{x}, \bar{x}_0$ | = Stratford length parameters, Eqs. (4) and (5) |
| $\Gamma$ | = circulation |
| $\rho$ | = air density |

*Subscripts*

| | |
|---|---|
| te | = trailing edge |
| $\infty$ | = freestream |

## Introduction

LIEBECK[1-3] has designed a number of new airfoil sections for high lift and high lift-to-drag ratio. Adopting Stratford's pressure gradient criteria for a *turbulent* boundary layer,[7] he was able to formulate and hence prescribe a pressure distribution which 1) was everywhere continuous with a front and rear stagnation point, 2) represented attached flow, and 3) was optimized for high lift. The airfoil shape was found by a suitable inverse method. The Liebeck procedure, when adapted to the design of realistic shapes, has been substantiated by wind-tunnel tests. Central to this design procedure is the premise that a turbulent boundary layer will always exist at the rear of the upper surface of an airfoil which is required to work over a large range of incidence at normal flight Reynold's numbers.

Although this enquiry was prompted by an interest in low Reynolds number flights, or flows, where the advantage of a turbulent boundary may not be available, the question of the existence, shape, and performance of airfoils in the limiting situation of fully laminar flow is believed to be of basic interest and significance if only because it assists in establishing new design objectives and constraints.

The question is, therefore, what results would be obtained by imposing Stratford's pressure gradient criteria for a fully laminar boundary layer? If a solution exists, the corresponding shapes and a measure of their performance are sought, under the same constraints (1-3) as Liebeck, above.

## Optimized Velocity Distribution

The lift produced by an airfoil section is given by

$$\ell = \rho \Gamma V_\infty \tag{1}$$

where

$$\Gamma = \int v \cdot ds \tag{2}$$

and $s$ is defined in Fig. 1. The velocity distribution $v(s)$ around the airfoil can be represented by two distributions, $v_u(s)$ and $v_\ell(s)$, corresponding to the upper and lower surfaces of the airfoil. Hence

$$\Gamma = \int_0^{s_p} v_\ell ds + \int_{s_p}^{s_{te}} v_u ds \tag{3}$$

Maximum lift requires that the front stagnation point be as far back as possible and that the velocities on the upper/lower surfaces be as high/low as possible. So as to enclose maximum area, the velocity distribution for the upper surface leading edge region, will have a flat rooftop, while the pressure recovery portion of the airfoil will be defined by Stratford's laminar boundary layer criteria. The distribution for the lower surface, on the other hand, is obtained from

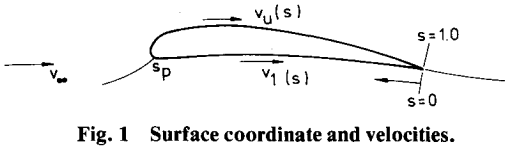


**Fig. 1 Surface coordinate and velocities.**

Received July 13, 1981; revision received Oct. 2, 1981. This paper is declared a work of the U.S. Government and therefore is in the public domain.

*Research Engineer, School of Mechanical and Industrial Engineering.

†Visiting Research Professor, Aerospace Engineering Department. On leave from School of Mechanical and Industrial Engineering, University of New South Wales. Member AIAA.

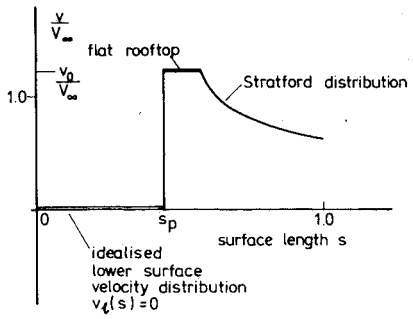


**Fig. 2 Idealized velocity distribution optimized for maximum lift.**

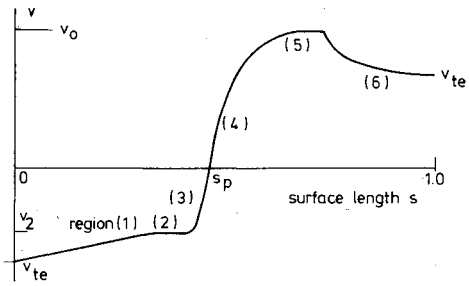


**Fig. 3 Representation of velocity distribution by six regions.**

minimization of the integral

$$\int_0^{s_p} v_l \mathrm{d}s$$

hence suggesting an idealized distribution of $v_l(s)=0$. Combining the two distributions for the upper and lower surfaces leads to Liebeck's idealized velocity distribution around the airfoil optimized for maximum lift[2] and is shown in Fig. 2. The discontinuities in shape to be seen there prevent a meaningful airfoil from being defined, however, so that modification will be necessary.

A practical velocity distribution has been defined by identifying six regions over the airfoil contour total length (which is set to unity), as shown in Fig. 3. The acceleration regions 3 and 4 are represented by one of four mathematical functions: linear, elliptic, parabolic, or sinusoidal. Region 6 is the Stratford region, while the remaining three regions are linear. For the elliptic case, a modification very near the stagnation point in the form of a finite slope is made in order to remove the infinite slope, which would otherwise result. The lower surface distribution (regions 1, 2, and 3) is matched to the upper surface distribution (regions 4, 5, and 6) by slope continuity at the front stagnation point and by a common velocity at the trailing edge, $v_{te}$, to satisfy the Kutta circulation constraint.

The Stratford criteria for minimum skin friction in a flat plate laminar boundary layer is given as[6]

$$\bar{C}_p = 0.2369[1.013\ \ell n(\bar{x}/\bar{x}_0) - 0.013(\bar{x}/\bar{x}_0 - 1)]^{2/3} \quad (4)$$

where

$$\bar{x}_0 = \int_0^{x_0} \left(\frac{v}{v_0}\right)^5 \mathrm{d}x \quad (5)$$

$x$ is the actual distance from the beginning of the boundary layer, in this case from the stagnation point. $\bar{x}$ is the effective distance from the beginning of the boundary layer when a favorable pressure gradient is present, while $\bar{x}_0$ is that value of $\bar{x}$ at the peak velocity value $v_0$. $\bar{C}_p$ is defined as

$$\bar{C}_p = \frac{p - p_0}{\frac{1}{2}\rho v_0^2} \quad (6)$$

and relates to the usual pressure coefficient $C_p$ by the expression

$$C_p = (v_0/V_\infty)^2(\bar{C}_p - 1) + 1 \quad (7)$$

The surface velocity is given by the Bernoulli expression

$$v(s) = [1 - C_p(s)]^{1/2} \quad (8)$$

Unlike the Stratford criteria for a turbulent boundary layer, the Reynolds number does not appear here. The immediate implications of this are that 1) laminar flow conditions must always prevail, and 2) a critical Reynolds number exists.

The upper surface velocity distribution is formulated by matching the acceleration regions 4 and 5 to the Stratford region 6. This is achieved by means of Eq. (5), which yields analytical solutions for $\bar{x}_0$ when either of the four leading edge velocity distributions is substituted. The unknown quantity $v_0$ drops out in Eq. (5) by cancellation. It is found from Eq. (7), which on rearranging gives

$$\frac{v_0}{V_\infty} = \left(\frac{C_p - 1}{\bar{C}_p - 1}\right)^{1/2} \quad (9)$$

Next, it is necessary to assign a value for $C_p$, at one point on the airfoil. A suitable location is the trailing edge, where typical values are $C_{p_{te}} \simeq 0.02\text{-}0.25$. $\bar{C}_{p_{te}}$ is obtained from Eq. (4), and hence $v_0$ follows.

Optimization of the upper surface distribution for maximum lift requires that the length of region 4 be kept as small as possible. Note that as this length approaches zero, the ideal distribution of Fig. 2 is realized. For small but realistic lengths of region 4, all four leading edge velocity distributions were found to give approximately the same low peak velocity value of $v_0 \simeq 1.3$ and a corresponding low flat rooftop length of approximately 4% of the surface length. Compare these values with those of Liebeck[1] using Stratford's turbulent boundary layer criterion, where $v_0$ is given as approximately 2.0, with the flat rooftop length approximately 20%.

The lower surface velocity distribution is arbitrarily specified but kept as low as possible so as to maximize lift. It is also made to continuously accelerate from the stagnation point to $v_{te}$, thus maintaining a favorable pressure gradient.

It now only remains to determine a suitable combination of the six regions which generate maximum possible lift for a closed airfoil. Finally, to find the section shape, an inverse program using Green's third identity was developed following the least-squares linearization technique formulated by Bristow.[4,5]

## Results and Discussion

Attention was first given to generating symmetrical shapes. This approach reduced the number of design variables and therefore helped in the initial understanding of the solutions. It was found that the slope of the leading edge velocity distribution controls the nose radius, and consequently has a bearing on the maximum thickness of the airfoil. The potential flow around a circular cylinder provides a simple demonstration of this (Fig. 4). The effect was found to be quite pronounced with relatively large nose radii resulting from small slope changes. The length of the flat rooftop did not appear to have a strong bearing on the airfoil shape excepting, however, the location of maximum thickness. The trailing edge velocity $v_{te}$ is specified as high as possible so as to obtain high lift. However, as its value approached unity, the trailing edge angle would approach the potential flow value of zero and thus develop an unacceptable cusp. A suitable value for $v_{te}$ was found to be 0.97. Figure 5 shows a symmetrical airfoil which has been designed with a sinusoidal leading edge velocity distribution. Solutions for the other

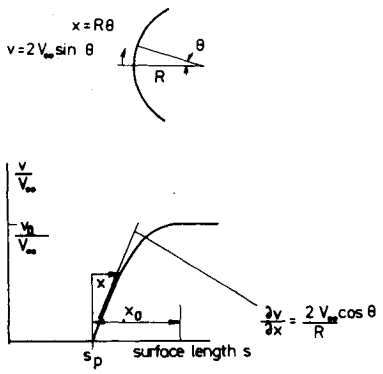


**Fig. 4 Relation between nose radius and leading edge velocity gradient.**

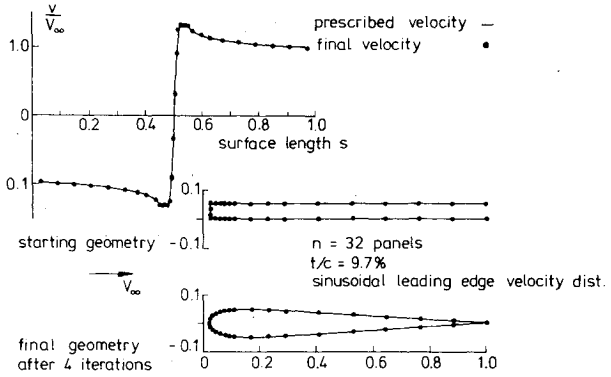


**Fig. 5 Symmetrical fully laminar airfoil.**

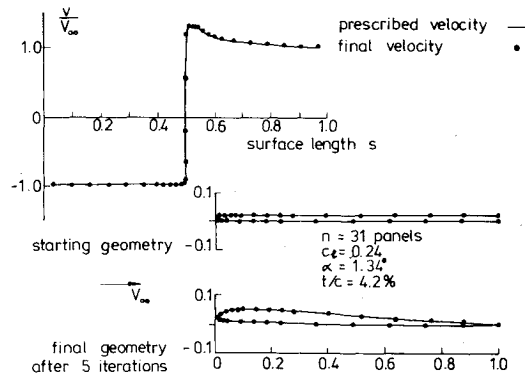


**Fig. 6 Cambered fully laminar airfoil.**

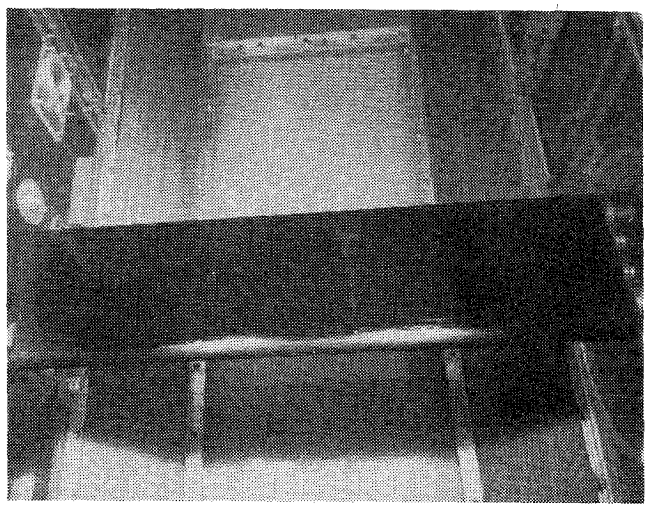

**Fig. 7 Wind-tunnel test of symmetric fully laminar airfoil; $Re = 166{,}000$, $t/c = 9.7\%$, $T = 0.2\%$. Freestream direction from bottom to top.**

leading edge velocity distributions were similar in appearance except for the nose region. The airfoils were found to have thicknesses approximately 8-10%, and a maximum located between 10-15% of the chord. NACA 4 and 5 digit series sections have their maximum thickness located at 30% of the chord. Although the airfoil in Fig. 5 is well defined, it has no operating range of incidence. Any deviation from zero incidence will cause laminar separation.

In contrast to symmetrical cases, cambered shapes were far more difficult to produce. Here the circulation was very sensitive to small changes in the various prescribed velocity distributions. The front stagnation point was found to be restricted in the range 0.498-0.5. It was generally found that, of the four mathematical acceleration functions, the elliptic leading edge velocity distribution was better able to match the prescribed velocities by providing the steepest initial velocity rise of the four cases, and good round-off at the top. This allowed a smaller nose radius to be formed so that the resulting section would not be thick, and therefore could more easily be accommodated between the prescribed upper and lower surface velocities. The other distributions tended to produce more rounded noses with the result that the final velocity would overshoot the prescribed values for either the upper or the lower surface. Attempts to produce a smaller nose radius by steepening the velocity slope resulted in leading edge flow conditions which could no longer be matched to the trailing edge closure condition. Figure 6 shows a cambered section designed with an elliptic and linear velocity distribution for the upper and lower leading edge, respectively. The lift coefficient is given as 0.24 at an incidence of 1.4 deg and the thickness is 4.2%, occurring at 18% chord.

Based on the Stratford distribution, the above represents an upper limit for fully laminar flow shapes. These small values of lift and incidence represent a very limited range under which such sections can operate. Although this study has been restricted by the nature of the allowable velocity distributions, various combinations of the four leading edge distributions and lengths of the six regions were prescribed and tested, but none produced a superior section.

## Experiment

A simple experiment to test for the presence of a fully attached laminar boundary layer was performed on a model of the 9.7%-thick symmetric section of Fig. 5. The coordinates were derived on a PDP 11/60 digital computer and fitted to a cubic spline curve. The smoothed section coordinates were then fed into a MAKINO FNC105-A numerically controlled mill which machined the profile. The constant chord model was covered with a flat black paint so as to prepare the surface for the liquid film flow visualization technique of Ref. 8. Sanding blocks with the reverse airfoil surface shape were also machined in order to ensure the correct surface shape during final finish after painting. The model was tested at the University of New South Wales in a $0.46 \times 0.46$-m ($18 \times 18$ in.) wind tunnel ($T = 0.2\%$). The model span was 0.46 m (18 in.), the chord was 0.12 m (4.72 in.), and the thickness was 11.7 mm (0.461 in.). Tunnel blockage was 2.5%.

Initial observations by means of tufts indicated steady flow over the airfoil. When a small incidence was applied (~3 deg), total separation along the whole pressure recovery length occurred, consistent with the behavior of Stratford type boundary layers. The liquid used for the boundary layer flow visualization tests at zero incidence was heating

kerosene. To contrast between a laminar and turbulent boundary layer, two artificial turbulent spots were located at approximately 5 and 55% chord positions. A series of runs were made at different Reynolds numbers and photographs taken. In taking the photographs, even lighting was obtained except at the leading edge regions, which are shiny owing to light reflection, and the slightly dark span ends owing to shadows. In the photograph (Fig. 7), for a Reynolds number of 166,000, turbulence in the wall region is also evident. Away from the walls, however, the only dry regions are the wedge shaped regions behind the turbulent spots. The boundary layer, therefore, over the whole of the remainder of the wing is laminar. The turbulence from the midchord spot, as can be seen, appears close to the trailing edge. The distance in between represents the amplification distance from the spot before instability in the layer is reached. At a lower Reynolds number of 125,000, turbulence from the midchord spot disappeared. The front turbulent spot still caused transition, however, owing to the severe initial Stratford gradient which the boundary layer must first encounter. At a Reynolds number of 83,000, the amplification distance from the front spot, before instability in the layer is reached, is approximately 80% of the chord. Finally, below Reynolds numbers of 83,000, no turbulence was evident. On the other hand, at a Reynolds number of 208,000, transition to turbulent flow occurred at about 65% chord over most of the span.

The stability of the boundary layer was found to be most critical at the front portion of the airfoil, where the boundary layer first encounters the initial severe Stratford gradient. If the airfoil was offset slightly from zero freestream incidence, local reverse flow would occur in this region. At the same time flow reattachment was observed just downstream, suggesting the presence of a leading edge separation bubble. From the above flow observations it would appear that a redesign of the flat rooftop region of the airfoil is desirable. This would be in the form of a better rounding of the velocity distribution there, and a gentler easing of the boundary layer into the initial severe Stratford gradient. It is noted that Liebeck incorporated these features in his design of turbulent boundary layer airfoil sections.

## Conclusions

Laminar flow airfoils have been designed and realistic shapes obtained. Their range of performance, however, is very limited with the maximum angle of attack and lift coefficient being in the order of 1.3 deg and 0.24, respectively. Experimental observations, by means of a liquid film test, have confirmed the presence of a laminar boundary layer over the whole airfoil for Reynolds numbers up to 166,000. Beyond this, transition to a turbulent boundary layer occurred. For Reynolds numbers below 83,000, the boundary layer remained laminar despite surface roughness, but remained attached only if the incidence was small enough to prevent separation. The thicknesses ranged from 4 to 10% with the position of maximum thickness between 10 and 20% chord. Maximum tolerable camber was 10% at 15% chord.

## References

[1] Liebeck, R.H., "A Class of Airfoils Designed for High Lift in Incompressible Flow," *Journal of Aircraft,* Vol. 10, Oct. 1973, p. 610.

[2] Liebeck, R.H. and Ormsbee, A.I., "Optimization of Aerofoils for Maximum Lift," *Journal of Aircraft*, Vol. 7, Sept. 1970, p. 409.

[3] Liebeck, R.H., "Design of Subsonic Airfoils for High Lift," *Journal of Aircraft,* Vol. 15, Sept. 1978, p. 547.

[4] Bristow, D.R., "A New Surface Singularity Method for Multi-Element Airfoil Analyses and Design," AIAA Paper 76-20, 1976.

[5] Bristow, D.R., "Improvements in Surface Singularity Analyses and Design Methods," NASA CP-2045, Vol. 1, Part 1, March 1978.

[6] Stratford, B.S., "Flow in the Laminar Boundary Layer near Separation," A.R.C., R&M 3002, Nov. 1954.

[7] Stratford, B.S., "The Prediction of Separation of the Turbulent Boundary Layer," *Journal of Fluid Mechanics*, Vol. 5, Jan. 1959, pp. 1-16.

[8] Gray, W.E., "A Simple Visual Method of Recording Boundary Layer Transition," R.A.E. Technical Note Aero. 1816, Aug. 1946.